Comput Mech (2014) 54:489–502
DOI 10.1007/s00466-014-1001-9

ORIGINAL PAPER

Modeling of dynamic crack branching by enhanced extended finite element method

Dandan Xu · Zhanli Liu · Xiaoming Liu · Qinglei Zeng · Zhuo Zhuang

Received: 11 December 2013 / Accepted: 19 February 2014 / Published online: 13 March 2014

Abstract The conventional extended finite element method (XFEM) is enhanced in this paper to simulate dynamic crack branching, which is a top challenge issue in fracture mechanics and finite element method. XFEM uses the enriched shape functions with special characteristics to represent the discontinuity in computation field. In order to describe branched cracks, it is necessary to set up the additional enrichment. Here we have developed two kinds of branched elements, namely the "element crossed by two separated cracks" and "element embedded by a junction". Another series of enriched degrees of freedom are introduced to seize the additional discontinuity in the elements. A shifted enrichment scheme is used to avoid the treatment of blending element. Correspondingly a new mass lumping method is developed for the branched elements based on the kinetic conservation. The derivation of the mass matrix of a four-node quadrilateral element which contains two strong discontinuities is specially presented. Then by choosing crack speed as the branching criterion, the branching process of a single mode I crack is simulated. The results including the branching angle and propagation routes are compared with that obtained by the conventionally used element deletion method.

D. Xu · Z. Liu (✉) · Q. Zeng · Z. Zhuang (✉)
Applied Mechanics laboratory, Department of Engineering Mechanics, School of Aerospace,
Tsinghua University, Beijing 100084, China
e-mail: liuzhanli@tsinghua.edu.cn

Z. Zhuang
e-mail: zhuangz@tsinghua.edu.cn

X. Liu
LNM, Institute of Mechanics, Chinese Academy of Sciences,
Beijing 100190, China

Keywords XFEM · Dynamic fracture mechanics · Mass lumping · Crack branching

1 Introduction

Crack branching is a phenomenon frequently observed in conjunction with dynamic fracture in brittle materials [1–3]. During the branching process the propagating crack often departs from its original straight trajectory and splits into two or more branches. This is widely observed in various natural and engineering phenomena. For example, the crack propagating and branching is frequently found in the earthquake rupture of rock faults and in the pressured gas pipeline. The dynamic fault branching is commonly concerned and studied [4,5]. The dynamic crack branching is an attractive topic because of its importance in understanding the failure of engineering structures and some natural disasters. In the past decades, there are a number of experiments, theoretical models, and numerical simulations performed to understand the dynamic fracture as well as crack branching.

A lot of researches are carried out to study the theory and mechanism of crack branching, but a generally accepted explanation for crack branching and a reliable branching criterion are still lacking. Fineberg [6] observes dynamic crack propagation, and finds that cracks in brittle material have terminal speed far below the Rayleigh wave speed. The crack loses stability when the speed exceeds a critical value v_c, which depends neither on the applied stress nor on the geometry of the specimen. Above v_c, the crack speed has strong oscillation and the original smooth crack surface becomes rough, consequently some micro-branches can be found. Yoffe [7] focuses on the asymptotic stress field ahead of a dynamic propagating crack, and the stress solution gives an explanation for crack branching, but the criti-

cal velocity of the theoretical prediction is higher than that from experiments. Eshelby [8] considers the energy-based approaches and proposes that the energy flux into the two branching crack tips equals to the energy required to open the material and create new surfaces as a result of this propagation. Using Eshelby's approach, Adda-Bedia [9] studies the dynamic stress intensity factors immediately after branching under plane loading configurations, and shows that the branching of a single propagating crack under mode I loading is energetically possible when its speed exceeds a threshold value. Martínd et al. [10] indicates that branching can be triggered by two different mechanisms, namely the kinematics of the strain field and back-reflected surface waves traveling on the crack tip. Katzav et al. [11] uses the Griffith energy criterion and the principle of local symmetry to predict the critical velocity for branching. Though being studied for several decades, the dynamic crack branching is still an open question.

How to numerically model the dynamic branching is also a challenge issue. In atomistic models, cracks can branch without a specific criterion [12]. Particle-type models [13] are also capable of simulating crack branching. However, these methods are not able to capture the crack speed and predict the branching angle correctly. Xu and Needleman [14] use finite element with the interelement cohesive crack model to examine multiple dynamic crack branching problems, and give the numerical results qualitatively in according with a variety of experiment observations on fast crack growth in brittle solids. Ha [15] uses peridynamic analysis to study the dynamic crack propagation and branching. In the method no special criteria for crack propagation and branching are used, which is obtained as a part of solution. Song and coworkers [16] study crack instabilities in a brittle material with a meshfree cracking particle method, and the microcrack branching is computed. Recently a phase field model of crack is widely used to study fracture problems. The advantage of this method is that it does not require the numerical tracking of discontinuity in the displacement. But this method needs a fairly fine mesh to obtain an ideal solution. Henry [17] use a phase field model of crack propagation to study the dynamic branching instability in the case of in-plane loading in two dimensions. Borden et al. [18] introduce phase field method to study the behavior of dynamic model by performing a number of two and three dimensional numerical experiments including the dynamic crack branching.

The extended finite element method (XFEM), which was put forward in 1999 [19,20], is an efficient numerical method on solving fracture mechanics, especially the problems of crack arbitrary propagation. The basic idea of XFEM is to introduce the enriched shape functions with special characteristics to represent the discontinuity in the calculation field. In XFEM, the mesh boundary does not have to coincide with the crack surface, so a structure mesh can be used for a complex crack growth, and re-meshing is not necessary when the crack propagates. The phantom node method which is a simplified adaption of XFEM is also widely used to model various 2D [21] and 3D [22] fracture problems. The studies of crack branching modeling using XFEM are still limited because of its complexity. Daux et al. [23] develops a methodology that constructs the enriched approximation based on the interaction of the discontinuous geometric features and calculates the stress intensity factor of static cracks with multiple branches. While it is only used for static branched cracks, the crack propagation and dynamic branching process are not taken into account. To deal with dynamic branching process, the construction of mass matrix for an element containing branched cracks is necessary. Belytschko et al. [24] introduce the loss of hyperbolic as the criterion of dynamic crack propagation, and use XFEM to deal with the discrete discontinuity. The method is applied to several dynamic crack growth problems including crack branching. In the simulation, the element in which the branching occurs is simply deleted because of difficulties in the enrichment. Song et al. [25] compare three different finite element methods including XFEM for dynamic crack propagation in brittle materials, and study the performance of these methods. Song et al. [21] simulate crack branching using the phantom nodes method which is a transformation of XFEM. The stress in elements which contain more than one crack is simply set to zero to simulate branched cracks. However, simply deleting the elements containing branched cracks is just an expedient and the accuracy and feasibility needs to be further demonstrated. A new cracking node method for modeling discrete cracks based on XFEM is also demonstrated with dynamic fracture problems including crack branching by Song et al. [26]. In the above all, the branching criterion, crack geometry description and construction of mass matrix for the branched element remain the challenge issues of modeling dynamic crack branching by XFEM.

In this paper, an enhanced XFEM is used to simulate dynamic crack propagating and branching. Additional enriched shape functions and the corresponding degrees of freedom are introduced to seize the discontinuity in the element which contains the junction of a branched crack. A shifted formulation of enrichment function makes it more convenient to deal with the blending element, but brings more difficulties in constructing the diagonal mass matrix for the branched element. A modified mass lumping scheme is deduced based on the principle of kinetic energy conservation for the element with a shifted enrichment. As one of key steps in the modeling of dynamic crack branching, the criterion is necessary but not unique. To the author's knowledge, it is difficult to find a generally accepted crack branching criterion. In this paper, according to the theoretical stress field near a fast propagating crack tip referring to Yoffe's solution, we analyze the normalized circumferential stress distribution

near the tip and propose a crack speed based branching criterion. By combining the criterion and the XFEM algorithm, the branching process of moving crack can be successfully simulated.

The paper is organized as follows. Section 2 describes the governing equations of the problem, and the XFEM framework including the enrichment scheme for crack with branches is introduced. Section 3 describes the lumping scheme of the mass matrix. Then criterion of crack branching used in the simulation is introduced in Sect. 4. Some numerical studies are provided in Sect. 5 to validate the accuracy and ability of the crack branching modeling. Finally, a summary is given in Sect. 6.

2 Governing equations and XFEM formulation

In this section, the governing equations are briefly reviewed for linear elastic fracture mechanics. Then the formulation of XFEM, especially the branching enrichment, is described in detail.

2.1 Governing equations

The governing equation in the Lagrangian coordinate system is

$$\frac{\partial P_{ji}}{\partial X_j} + \rho_0 b_i = \rho_0 \ddot{u}_i, \quad \text{in } \Omega_0 \tag{1}$$

where P is nominal stress, b is body force, ρ_0 is density corresponding to the initial configuration and the superposed dots denote material time derivative. Considered the domain Ω with boundary of Γ, it is composed of the sets Γ^{u}, Γ^{t}, and Γ^{c}, respectively, as shown in Fig. 1. Such that $\Gamma = \Gamma^{\mathrm{u}} \cup \Gamma^{\mathrm{t}} \cup \Gamma^{\mathrm{c}}$. The prescribed displacements are imposed on Γ^{u}, tractions are imposed on Γ^{t}, while Γ^{c} is the crack surface and is assumed to be traction-free.

Boundary and initial conditions are given below:

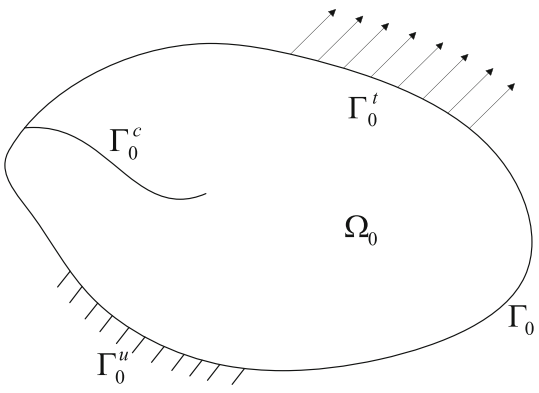

Fig. 1 Initial configuration

Displacement boundary condition, $u_i = \bar{u}_i, \quad \text{on } \Gamma_0^u$;
Force boundary condition, $n_j^0 P_{ji} = \bar{t}_i^0, \quad \text{on } \Gamma_0^t$;
Strong discontinuity, $n_j^{0+} P_{ji}^+ = n_j^{0-} P_{ji}^- = 0, \quad \text{on } \Gamma_0^c$;
Initial conditions, $\dot{u}_i(0) = \dot{u}_{i0}, \quad P_{ij}(0) = P_{ij0}$.

Multiply δu on both sides of Eq. (1) and integrate on initial configuration. The integral form of equation is obtained as

$$\int_{\Omega_0} \delta u_i \left(\frac{\partial P_{ji}}{\partial X_j} + \rho_0 b_i - \rho_0 \ddot{u}_i \right) \mathrm{d}\Omega_0 = 0. \tag{2}$$

Using integration by parts and the divergence theorem, we obtain the weak form of the governing equation as follow

$$\int_{\Omega_0} \left(\delta F_{ij} P_{ji} - \delta u_i \rho_0 b_i + \delta u_i \rho_0 \ddot{u}_i \right) \mathrm{d}\Omega_0 - \int_{\Gamma_0^t} \delta u_i \bar{t}_{i0} \mathrm{d}\Gamma_0 = 0 \quad \forall \delta u \in U_0 \tag{3}$$

where $U_0 = \left\{ \delta \boldsymbol{u}(\boldsymbol{X}) | \delta \boldsymbol{u}(\boldsymbol{X}) \in C^0, \ \delta \boldsymbol{u}(\boldsymbol{X}) = 0, \ \text{on } \Gamma_0^{\mathrm{u}}, \ \delta \boldsymbol{u} \right.$ discontinuous on $\left. \Gamma_0^{\mathrm{u}} \right\}$ is the test function.

2.2 Discretization and XFEM

In the XFEM framework, the displacement approximation is

$$\boldsymbol{u}^h(\boldsymbol{X}) = \sum_I N_I(\boldsymbol{X}) \boldsymbol{u}_I + \sum_J N_J(\boldsymbol{X}) \Phi_J(\boldsymbol{X}) \boldsymbol{q}_J \tag{4}$$

where I is a set of all nodes, and J is a set of the enriched nodes. $N_I(\boldsymbol{X})$ is the standard FEM shape function, $\Phi_J(\boldsymbol{X})$ is the enriched function, $\boldsymbol{u}_I$ is the standard degree of freedom, and $\boldsymbol{q}_J$ is the enriched degree of freedom associated with $\Phi_J(\boldsymbol{X})$. The variation of displacement is

$$\delta \boldsymbol{u} = \sum_I N_I(\boldsymbol{X}) \delta \boldsymbol{u}_I + \sum_J N_J(\boldsymbol{X}) \Phi_J(\boldsymbol{X}) \delta \boldsymbol{q}_J \tag{5}$$

By substituting Eq. (5) into Eq. (3), the momentum equation is obtained, which is solved to get the final results.

$$\begin{bmatrix} \boldsymbol{M}_{uu} & \boldsymbol{M}_{uq} \\ \boldsymbol{M}_{uq}^T & \boldsymbol{M}_{qq} \end{bmatrix} \begin{pmatrix} \ddot{\boldsymbol{u}} \\ \ddot{\boldsymbol{q}} \end{pmatrix} + \begin{bmatrix} \boldsymbol{K}_{uu} & \boldsymbol{K}_{uq} \\ \boldsymbol{K}_{uq}^T & \boldsymbol{K}_{qq} \end{bmatrix} \begin{pmatrix} \boldsymbol{u} \\ \boldsymbol{q} \end{pmatrix} = \begin{pmatrix} \boldsymbol{f}^{ext} \\ \boldsymbol{Q}^{ext} \end{pmatrix} \tag{6}$$

where $\boldsymbol{u}$ is the standard degree of freedom, while $\boldsymbol{q}$ is the enriched degree of freedom. $\boldsymbol{f}^{ext}$ is the external nodal force corresponding to $\boldsymbol{u}$, while $\boldsymbol{Q}^{ext}$ is the external nodal forces corresponding to $\boldsymbol{q}$. The mass matrix $\boldsymbol{M}$ and stiffness matrix $\boldsymbol{K}$ contain the standard term uu, the enriched term qq, and the coupled term uq, respectively, as shown in Eq. (6), which is solved by typical implicit Newmark − β method. More details can be found in our previous work in Refs.[27,28].

The most important part of XFEM is to choose proper enriched function. As mentioned above, in this method the crack can propagate across the element arbitrarily without

going along the element boundary, thus, some elements may be crossed by the crack, while the others contain crack tip. As the different position relationship between the element and the crack, the enrichment scheme is not the same. For different kinds of elements, the enriched function Φ_J has different forms to seize the characteristics of the discontinuity.

If an element is crossed by a crack, a Heaviside function is usually used as the enriched function. In this paper, a shifted form is adopted. The enriched function is selected as

$$\Phi_J(\boldsymbol{X}) = H(f(\boldsymbol{X})) - H(f(\boldsymbol{X}_J)) \tag{7}$$

where $H(\varphi)$ is the Heaviside function with the definition of

$$H(\varphi) = \begin{cases} 1, & \varphi \geq 0 \\ -1, & \varphi < 0 \end{cases} \tag{8}$$

and $f(\boldsymbol{X})$ is a signed distance function as

$$f(\boldsymbol{X}) = \min_{\overline{\boldsymbol{X}} \in \Gamma_0^c} \left\| \boldsymbol{X} - \overline{\boldsymbol{X}} \right\| \cdot \text{sign}(\text{n}^+ \cdot (\boldsymbol{X} - \overline{\boldsymbol{X}})) \tag{9}$$

If an element is embedded by a crack tip, the following enriched function is used

$$\Phi_J(\boldsymbol{X}) = b(\boldsymbol{X}) - b(\boldsymbol{X}_J) \tag{10}$$

where $b(\boldsymbol{X})$ is a linear combination of the following basis

$$b(\boldsymbol{X}) = \left[\sqrt{r} \sin\frac{\theta}{2}, \sqrt{r} \sin\frac{\theta}{2} \sin\theta, \sqrt{r} \cos\frac{\theta}{2}, \sqrt{r} \cos\frac{\theta}{2} \sin\theta \right] \tag{11}$$

This basis is borrowed from the solution of linear elastic fracture mechanics so that the singularity at the crack tip can be obtained.

More details about the XFEM can be found in Refs.[19, 20,29,30].

2.3 Branching enrichment

In the above, the enrichment scheme of a single crack in a two-dimensional body is introduced, while the enrichment should be improved when it meets the branched cracks. Daux et al. [23] introduce the discontinuous functions for modeling branched cracks. A junction function is used as the additional enriched function. Zi et al. [31] combine two step enrichments to implement the junction of two cracks for the problem of growing multiple cracks. Based on this idea, a shifted form is developed in this paper and the details are introduced in the following.

When modeling the branched cracks, two kinds of new enriched elements are considered. They are the element crossed by two separated cracks and the element embedded by a junction, as shown in Fig. 2a, b, respectively. In these two kinds of enriched elements, the approximate displacement field is needed to be improved, and the description for the additional crack is necessary.

If there are two separate cracks existing in the same element, only one series of enriched degrees of freedom is not enough to describe the discontinuous feature of the element displacement field. One more enrichment is necessary to seize the additional discontinuity in the element. Another signed displacement function is introduced to describe the position of the second crack. The displacement field can be approximately expressed as

$$\begin{aligned} \boldsymbol{u}^h(\boldsymbol{X}) = & \sum_{I=1}^{4} N_I(\boldsymbol{X}) \boldsymbol{u}_I \\ & + \sum_{J=1}^{4} N_J(\boldsymbol{X}) \left[H(f^{\text{I}}(\boldsymbol{X})) - H(f^{\text{I}}(\boldsymbol{X}_J)) \right] \boldsymbol{q}_J^{\text{I}} \\ & + \sum_{K=1}^{4} N_K(\boldsymbol{X}) \left[H(f^{\text{II}}(\boldsymbol{X})) - H(f^{\text{II}}(\boldsymbol{X}_K)) \right] \boldsymbol{q}_K^{\text{II}} \end{aligned} \tag{12}$$

where $f^{\text{I}}(\boldsymbol{X})$ and $f^{\text{II}}(\boldsymbol{X})$ are the signed distance functions to the first (red solid line in Fig. 2a) and second (green dashed line in Fig. 2a) crack, respectively. $\boldsymbol{q}_J^{\text{I}}$ and $\boldsymbol{q}_K^{\text{II}}$ are the enriched degrees of freedom associated with two cracks. The first crack is enriched as if the secondary crack is absent, and the second item of right hand side of Eq. (12) stands for it. Similarly, the second crack is enriched almost as if the first crack is absent, and the third item of right hand side of Eq. (12) stands for it. By putting them together, the two cracks in the same element can be described and modeled.

The element containing a junction is the element in which the crack branching occurs as shown in Fig. 2b. The number of degrees of freedom is the same as the element with two separate cracks, and the enrichment scheme is also similar to each other. Besides the original enrichment, a junction function is defined in this element. The approximation of the displacement field is expressed as

$$\begin{aligned} \boldsymbol{u}^h(\boldsymbol{X}) = & \sum_{I=1}^{4} N_I(\boldsymbol{X}) \boldsymbol{u}_I \\ & + \sum_{J=1}^{4} N_J(\boldsymbol{X}) \left[H(f^{\text{I}}(\boldsymbol{X})) - H(f^{\text{I}}(\boldsymbol{X}_J)) \right] \boldsymbol{q}_J^{\text{I}} \\ & + \sum_{K=1}^{4} N_K(\boldsymbol{X}) \left[J(\boldsymbol{X}) - J(\boldsymbol{X}_K) \right] \boldsymbol{q}_K^{\text{II}} \end{aligned} \tag{13}$$

where $J(\boldsymbol{X})$ is the junction function with the definition of

$$J(\boldsymbol{X}) = \begin{cases} H(f^{\text{I}}(\boldsymbol{X})), & \text{on the side without branch} \\ H(f^{\text{II}}(\boldsymbol{X})) & \text{on the side with branch} \end{cases} \tag{14}$$

We regard the main crack and one of the two branches as the first crack (red solid line in Fig. 2b), and $f^{\text{I}}(\boldsymbol{X})$ is the signed distance function corresponding to it. The other branch is the second crack (green dashed line in Fig. 2b),

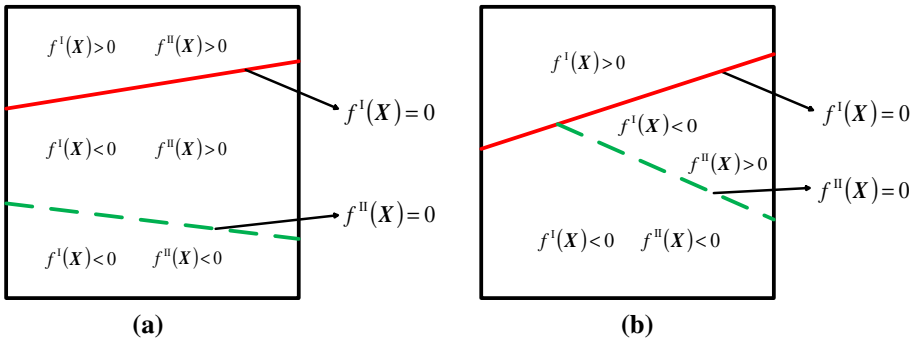

Fig. 2 Distance funtions: **a** element crossed by two separate cracks; **b** element embedded by a junction

and $f^{\mathrm{II}}(\boldsymbol{X})$ is the signed distance function corresponding to it. It is worth mentioning that in the definition of $J(\boldsymbol{X})$, the side with branch refers to the region where $f^{\mathrm{I}}(\boldsymbol{X}) < 0$ as shown in Fig. 2b. The fundamental concept of the junction function $J(\boldsymbol{X})$ has certain similarity with the contribution of the junction enrichment when one crack approaches and touches another crack, which is proposed in Ref. [31]. By applying the new enrichment to XFEM procedure, the cracks with branches can be modeled.

It is very convenient to treat the blending element with this shifted formulation of enrichment function. However, it brings more difficulties in constructing the diagonal mass matrix for the branched element since a sophisticated lumping scheme for shifted formulation is still lacking at present. A modified mass lumping scheme is deduced based on the principle of kinetic energy conservation for the branched element, which is discussed in the following section.

3 Lumping scheme of mass matrix

The lumped mass matrix is commonly used in the dynamic simulation. In this section, the lumping scheme of the mass matrix corresponding to the modified XFEM formulation is introduced in details. It is difficult to construct the lumped mass matrix in the discontinuous element when the shifted multi and junction enrichments are used. Here we construct the lumped mass by following the basic principle to guarantee that the discrete kinetic energy is exact for some special motions. The definition of the mass matrix based on shifted enriched shape function is introduced, which is started from one dimension (1D) and then extended to 2D problem.

3.1 One dimension problem

Firstly, take the 1D problem as an example to show the detail of the mass lumping scheme. We assume the diagonal mass matrix of the element is $\boldsymbol{M} = \mathrm{diag}\,[m_1 \;\; m_2 \;\; m_1' \;\; m_2']$, where m_1 and m_2 are masses corresponding to the standard nodes in the element, while m_1' and m_2' are masses corresponding to the enriched nodes. In order to determine $\boldsymbol{M}$, two motion modes are selected.

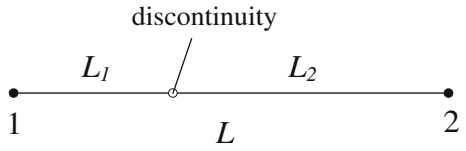

Fig. 3 Schematic of 1D element

The first one is the rigid body motion with a constant velocity of $\dot{\bar{u}}$, thus the velocity of the element is $\dot{u} = \dot{\bar{u}}$. Considering one discontinuity in the element, as shown in Fig. 3, the displacement interpolation of the element is

$$u(x) = \sum_{I=1}^{2} N_I(x) u_I + \sum_{J=1}^{2} N_J(x)\,[H(f(x)) - H(f(x_J))]\,q_J \tag{15}$$

The velocities on the nodes are supposed $\dot{u}_I = \dot{\bar{u}}$ and $\dot{q}_I = 0\,(I = 1, 2)$. The approximate kinetic energy is

$$T^h = \frac{1}{2}\dot{\boldsymbol{u}}^T \boldsymbol{M} \dot{\boldsymbol{u}} = \frac{1}{2}\begin{bmatrix}\dot{\bar{u}} & \dot{\bar{u}} & 0 & 0\end{bmatrix}\begin{bmatrix} m_1 & 0 & 0 & 0 \\ 0 & m_2 & 0 & 0 \\ 0 & 0 & m_1' & 0 \\ 0 & 0 & 0 & m_2' \end{bmatrix}\begin{Bmatrix}\dot{\bar{u}} \\ \dot{\bar{u}} \\ 0 \\ 0\end{Bmatrix} = \frac{1}{2}(m_1 + m_2)\dot{\bar{u}}^2 \tag{16}$$

The exact kinetic energy is

$$T = \int \frac{1}{2}\rho \dot{\bar{u}}^2 \mathrm{d}x = \frac{1}{2}\dot{\bar{u}}^2 \int \rho \mathrm{d}x = \frac{1}{2} m \dot{\bar{u}}^2 \tag{17}$$

where m is the mass of whole element. Let $T^h = T$, we obtain

$$m_1 + m_2 = m \tag{18}$$

Equation (18) is the requirement of mass corresponding to the standard nodes, and we may assume

$$m_1 = m_2 = \frac{1}{2} m \tag{19}$$

The second motion mode is described by the velocities on the nodes as $\dot{u}_I = 0, \dot{q}_I = \dot{\bar{u}}$, unfortunately it is not of a specific physics meaning. The motion of the element is obtained from Eq. (15) as

$$\begin{aligned}\dot{u}(x) &= \sum_{I=1}^{2} N_I(x)\dot{u}_I + \sum_{J=1}^{2} N_J(x)\left[H(f(x)) - H(f(x_J))\right]\dot{q}_J \\ &= \left[H(f(x)) - \sum_{J=1}^{2} N_J(x)H(f(x_J))\right]\dot{\bar{u}} \end{aligned} \tag{20}$$

The approximate kinetic energy of this motion mode is

$$\begin{aligned} T^h &= \frac{1}{2}\dot{\boldsymbol{u}}^T \boldsymbol{M}\dot{\boldsymbol{u}} = \frac{1}{2}\begin{bmatrix} 0 & 0 & \dot{\bar{u}} & \dot{\bar{u}} \end{bmatrix} \begin{bmatrix} m_1 & 0 & 0 & 0 \\ 0 & m_2 & 0 & 0 \\ 0 & 0 & m_1' & 0 \\ 0 & 0 & 0 & m_2' \end{bmatrix} \begin{Bmatrix} 0 \\ 0 \\ \dot{\bar{u}} \\ \dot{\bar{u}} \end{Bmatrix} \\ &= \frac{1}{2}(m_1' + m_2')\dot{\bar{u}}^2 \end{aligned} \tag{21}$$

The exact kinetic energy is

$$\begin{aligned} T &= \int \frac{1}{2}\rho \dot{u}^2 \mathrm{d}x \\ &= \int \frac{1}{2}\rho \left\{ \sum_{J=1}^{2} N_J(x)\left[H(f(x)) - H(f(x_J))\right]\dot{\bar{u}} \right\}^2 \mathrm{d}x \\ &= \frac{1}{2}\dot{\bar{u}}^2 \int \rho \left[H(f(x)) - \sum_{J=1}^{2} N_J(x)H(f(x_J)) \right]^2 \mathrm{d}x \\ &= \frac{1}{2} m' \dot{\bar{u}}^2 \end{aligned} \tag{22}$$

where $m' = \int \rho \left[H(f(x)) - \sum_{J=1}^{2} N_J(x)H(f(x_J))\right]^2 \mathrm{d}x$ is the effective mass of the element in this motion mode. From $T^h = T$, we obtain the requirement of mass corresponding to the enriched nodes as

$$m_1' + m_2' = m' \tag{23}$$

For deciding the assignment of the mass, we consider the position of discontinuity in the element, and assign the mass matrix as following as

$$m_I' = \frac{L_I}{L} m', \quad I = 1, 2 \tag{24}$$

where L is the length of the element and L_I is the distance between the discontinuity and the I th node as shown in Fig. 4. The effective mass depends on the position of discontinuity in the element. In the following example, the motion mode and the diagonal mass are given specifically. We assume the discontinuity in the middle of the element as shown in Fig. 4. The shape functions are given by

$$N_1(x) = -\left(\frac{x}{L} - \frac{1}{2}\right), \quad N_2(x) = \frac{x}{L} + \frac{1}{2} \tag{25}$$

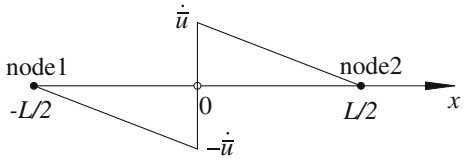

Fig. 4 Distribution of velocity

The velocity of element is

$$\begin{aligned} \dot{u}(x) &= N_1(x)u_1 + N_2(x)u_2 + N_1(x)[H(x) - H(x_1)]q_1 \\ &\quad + N_2(x)\left[H(x) - H(x_2)\right]q_2 \\ &= -\left(\frac{x}{L} - \frac{1}{2}\right)[H(x) + 1]\dot{\bar{u}} \\ &\quad + \left(\frac{x}{L} + \frac{1}{2}\right)[H(x) - 1]\dot{\bar{u}} \\ &= \begin{cases} \left(1 - \frac{2x}{L}\right)\dot{\bar{u}}, & x > 0 \\ \left(-1 - \frac{2x}{L}\right)\dot{\bar{u}}, & x < 0 \end{cases} \end{aligned} \tag{26}$$

The distribution of velocity is illustrated in Fig. 4.

In this case, the effective mass of element is

$$\begin{aligned} m' &= \int \rho \left[H(f(x)) - \sum_{J=1}^{2} N_J(x)H(f(x_J)) \right]^2 \mathrm{d}x \\ &= \int_{-\frac{L}{2}}^{\frac{L}{2}} \rho \left[H(f(x)) - \frac{2x}{L} \right]^2 \mathrm{d}x \\ &= \int_{-\frac{L}{2}}^{0} \rho \left(-1 - \frac{2x}{L}\right)^2 dx + \int_{0}^{\frac{L}{2}} \rho \left(1 - \frac{2x}{L}\right)^2 \mathrm{d}x \\ &= \frac{\rho L}{3} \end{aligned} \tag{27}$$

By using the shifted enriched function, the effective mass of an element with discontinuity does not equal to the exact mass of the whole element. The mass on the enriched nodes are

$$m_1' = m_2' = \frac{m'}{2} = \frac{\rho L}{6} \tag{28}$$

The mass on standard nodes are $m_1 = m_2 = \frac{1}{2}m = \frac{\rho L}{2}$. Thus the mass matrix of this element is

$$\boldsymbol{M} = \begin{bmatrix} \frac{\rho L}{2} & & & \\ & \frac{\rho L}{2} & & \\ & & \frac{\rho L}{6} & \\ & & & \frac{\rho L}{6} \end{bmatrix} \tag{29}$$

3.2 Two dimension problem

Following the basic idea of 1D problem, the scheme is extended to 2D problem. The element with two cracks is

considered, and the element with one crack or junction can be obtained by analogy. Four-node quadrilateral element is used here. In this kind of element, each node is enriched twice, so the number of degrees of freedom of the element increases to 24, and the size of the mass matrix is 24×24.

Assuming the mass of the standard nodes is m_J, where $J = 1, 2, 3, 4$ are the index of the nodes. The mass of the first set of enriched nodes is m'_J, $J = 1, 2, 3, 4$, and the mass of the second set of enriched nodes is m''_J, $J = 1, 2, 3, 4$. Three motion modes are required to determine the mass matrix.

Motion mode one is rigid body motion $\boldsymbol{u} = \dot{\bar{\boldsymbol{u}}}$, and the velocity on the nodes is $\boldsymbol{u}_I = \dot{\bar{\boldsymbol{u}}}, \dot{\boldsymbol{q}}_I^{\mathrm{I}} = 0, \dot{\boldsymbol{q}}_I^{\mathrm{II}} = 0$, respectively. The subscript I =1, 2, 3, 4 are the index of the nodes, and the superscript I and II indicate that they are the enrichments for the first and second crack inside the element, respectively. The discrete kinetic energy is given by

$$T^h = \frac{1}{2}(m_1 + m_2 + m_3 + m_4)\dot{\bar{\boldsymbol{u}}}^2 \tag{30}$$

while the exact kinetic energy is

$$T = \int \frac{1}{2}\rho \dot{\bar{\boldsymbol{u}}}^2 \mathrm{d}x = \frac{1}{2}\dot{\bar{\boldsymbol{u}}}^2 \int \rho \mathrm{d}x = \frac{1}{2} m \dot{\bar{\boldsymbol{u}}}^2 \tag{31}$$

From $T^h = T$, we obtain

$$m_1 + m_2 + m_3 + m_4 = m \tag{32}$$

where m is the mass of element. We assign the standard mass on the nodes to be equal to each other as follows

$$m_1 = m_2 = m_3 = m_4 = \frac{m}{4} \tag{33}$$

Motion mode two is defined on the velocities of the nodes as $\boldsymbol{u}_I = \boldsymbol{0}, \dot{\boldsymbol{q}}_I^{\mathrm{I}} = \dot{\bar{\boldsymbol{u}}}, \dot{\boldsymbol{q}}_I^{\mathrm{II}} = \boldsymbol{0}$, respectively. The discrete kinetic energy is

$$T^h = \frac{1}{2}(m'_1 + m'_2 + m'_3 + m'_4)\dot{\bar{\boldsymbol{u}}}^2 \tag{34}$$

The exact kinetic energy is

$$\begin{aligned} T &= \int \frac{1}{2}\rho \dot{\boldsymbol{u}}^2 \mathrm{d}x \\ &= \int \frac{1}{2}\rho \left\{ \sum_{J=1}^{4} N_J(\boldsymbol{X}) \left[H(f^{\mathrm{I}}(\boldsymbol{X})) - H(f^{\mathrm{I}}(\boldsymbol{X}_J)) \right] \dot{\bar{\boldsymbol{u}}} \right\}^2 \mathrm{d}x \\ &= \frac{1}{2}\dot{\bar{\boldsymbol{u}}}^2 \int \rho \left[H(f^{\mathrm{I}}(\boldsymbol{X})) - \sum_{J=1}^{4} N_J(\boldsymbol{X}) H(f^{\mathrm{I}}(\boldsymbol{X}_J)) \right]^2 \mathrm{d}x \\ &= \frac{1}{2} m' \dot{\bar{\boldsymbol{u}}}^2 \end{aligned} \tag{35}$$

where $m' = \int \rho \left[H(f^{\mathrm{I}}(\boldsymbol{X})) - \sum_{J=1}^{4} N_J(\boldsymbol{X}) H(f^{\mathrm{I}}(\boldsymbol{X}_J)) \right]^2 \mathrm{d}x$ and $T^h = T$, we obtain

$$m'_1 + m'_2 + m'_3 + m'_4 = m' \tag{36}$$

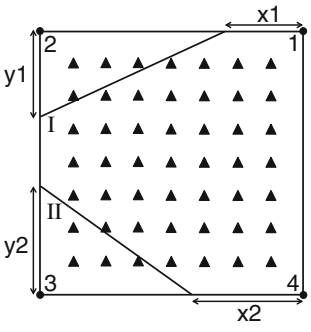

Fig. 5 Integration point distribution

The assignment scheme of the mass is

$$m'_J = \frac{n_{\mathrm{sub}J}^{\mathrm{int\,I}} \cdot m'}{n_{\mathrm{ele}}^{\mathrm{int}} \cdot n_{\mathrm{sub}J}^{\mathrm{nodeI}}}, \quad J = 1, 2, 3, 4 \tag{37}$$

Considering the first discontinuity in the element, $n_{\mathrm{sub}J}^{\mathrm{intI}}$ is the number of the integration points in the subdomain, which contains the J th node; $n_{\mathrm{ele}}^{\mathrm{int}}$ is the number of integration points in the whole element, and $n_{\mathrm{sub}J}^{\mathrm{nodeI}}$ is the number of nodes in the subdomain, which contains the J th node. The mass selection is a weight assignment based on the integration points. For example, the integration point schematic is illustrated in Fig. 5. In this element, $n_{\mathrm{ele}}^{\mathrm{int}} = 49$, $n_{\mathrm{sub1}}^{\mathrm{intI}} = n_{\mathrm{sub3}}^{\mathrm{intI}} = n_{\mathrm{sub4}}^{\mathrm{intI}} = 45$, $n_{\mathrm{sub2}}^{\mathrm{intI}} = 4$, and $n_{\mathrm{sub1}}^{\mathrm{nodeI}} = n_{\mathrm{sub3}}^{\mathrm{nodeI}} = n_{\mathrm{sub4}}^{\mathrm{nodeI}} = 3$, $n_{\mathrm{sub2}}^{\mathrm{nodeI}} = 1$. When consider about the first crack, the second crack is ignored.

The integral scheme is modified in each enriched element to ensure accurate integration. For each enriched element, the integration points are scattered uniformly and in the critical lengths of x and y directions, there must be at least two integration points. The critical length in x or y direction is defined as the shortest distance from the crossing point of the crack and element edge to the node. For example, in Fig. 5 the critical length of x direction is the minimum of x1 and x2, while the critical length of y direction is the minimum of y1 and y2.

Motion mode three is defined as $\boldsymbol{u}_I = \boldsymbol{0}, \dot{\boldsymbol{q}}_I^{\mathrm{I}} = \boldsymbol{0}, \dot{\boldsymbol{q}}_I^{\mathrm{I}} = \dot{\bar{\boldsymbol{u}}}$. It is similar with the condition of the first discontinuity. We can obtain the requirement of mass on the second set of enriched nodes as follow

$$m''_1 + m''_2 + m''_3 + m''_4 = m'' \tag{38}$$

where, $m'' = \int \rho \left[H(f^{\mathrm{II}}(\boldsymbol{X})) - \sum_{J=1}^{4} N_J(\boldsymbol{X}) H(f^{\mathrm{II}}(\boldsymbol{X}_J)) \right]^2 \mathrm{d}x$. The assignment of the mass on each node is based on the following formula and idea is the same as the former.

$$m''_J = \frac{n_{\mathrm{sub}J}^{\mathrm{int\,II}} \cdot m''}{n_{\mathrm{ele}}^{\mathrm{int}} \cdot n_{\mathrm{sub}J}^{\mathrm{nodeII}}}, \quad J = 1, 2, 3, 4 \tag{39}$$

where $n_{\mathrm{sub}J}^{\mathrm{int\,II}}$ and $n_{\mathrm{sub}J}^{\mathrm{nodeII}}$ are the number of integration points and the nodes of the subdomain cut by the second discon-

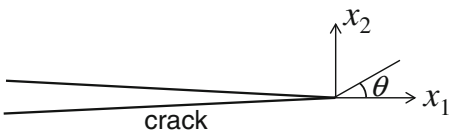

Fig. 6 Crack tip configuration

tinuity, respectively. At this time, the first discontinuity is ignored.

4 Criterion of crack branching

The crack propagation criterion and some fundamental concept of dynamic fracture mechanics are reviewed in this section. The criterion for dynamic crack branching is used based on the solution of Yoffe [7], which is applied for initiating crack branching and predicting branching angle.

4.1 Crack propagation criterion

In the quasi-static crack propagation for a mixed mode crack, as shown in Fig. 6, the maximum circumferential stress criterion is generally used. It assumes that the crack propagates perpendicular to the direction of the maximal circumferential stress, when the effective stress intensity factor along that direction reaches the fracture toughness.

For dynamic crack propagation, which is numerically simulated here, the propagation criterion has similar basic idea with the static condition. Firstly, we must check whether the crack is going to propagate using the criterion shown in Eq. (40).

$$\begin{aligned} &\text{if} \quad K_\theta^{\text{dyn}} < K_{Ic}, \quad \text{then} \quad V = 0 \\ &\text{else} \quad K_\theta^{\text{dyn}} = K_{ID}(V), \quad V > 0 \end{aligned} \tag{40}$$

where V is the propagation speed of the crack. If the effective stress intensity factor K_θ^{dyn} does not reach the fracture toughness K_{Ic}, the crack will not propagate, so the crack speed is zero; while if it reaches the critical value, the crack may start to propagate. For a steady propagating crack, the dynamic stress intensity factor equals to the dynamic fracture toughness $K_{ID}(V)$, which is related with the propagation speed of the crack. The direction of the maximum circumferential stress θ_c is calculated from Eq. (41). It is deduced from the stress field distribution near a steady moving crack tip, which is similar with the static case. Thus, the effective stress intensity factor K_θ^{dyn} on that direction can be obtained from Eq. (42).

$$\theta_c = 2\arctan\frac{1}{4}\left(\frac{K_I^{\text{dyn}}}{K_{II}^{\text{dyn}}} - \text{sign}\left(K_{II}^{\text{dyn}}\right)\sqrt{\left(\frac{K_I^{\text{dyn}}}{K_{II}^{\text{dyn}}}\right)^2 + 8}\right) \tag{41}$$

$$K_\theta^{\text{dyn}} = \cos^3\left(\frac{\theta_c}{2}\right)K_I^{\text{dyn}} - \frac{3}{2}\cos\left(\frac{\theta_c}{2}\right)\sin\theta_c K_{II}^{\text{dyn}} \tag{42}$$

The stress intensity factors can be calculated numerically by interaction integral method, and details can be found in Ref. [32]. The dynamic fracture toughness is obtained by the experiments. Unlike the static fracture toughness, the dynamic one is not constant, but varies with the crack speed V. As an approximation, we have the following equation describing the relationship between the dynamic fracture toughness and the crack propagation speed [30]

$$K_{ID}(V) = \frac{K_{Ic}}{1 - (V/c_R)^m} \tag{43}$$

where c_R is the Rayleigh wave speed. Here we choose $m = 1$, and obtain the following formula to estimate the crack propagation speed.

$$V = \left(1 - \frac{K_{Ic}}{K_\theta^{\text{dyn}}}\right)c_R \tag{44}$$

4.2 Crack branching criterion

Yoffe [7] gave the theoretical solution of displacement and stress field near the fast moving crack tip. The stress field distribution depends on the crack speed. For a moving mode I crack, the main terms of the stress field are given by

$$\sigma_{xx} = \frac{K_I(V)}{\sqrt{2\pi}}\frac{1+\alpha_2^2}{4\alpha_1\alpha_2 - \left(1+\alpha_2^2\right)^2}\left[\left(1+2\alpha_1^2-\alpha_2^2\right)\frac{\cos\frac{\theta_1}{2}}{\sqrt{r_1}} - \frac{4\alpha_1\alpha_2}{1+\alpha_2^2}\frac{\cos\frac{\theta_2}{2}}{\sqrt{r_2}}\right] \tag{45}$$

$$\sigma_{yy} = \frac{K_I(V)}{\sqrt{2\pi}}\frac{1+\alpha_2^2}{4\alpha_1\alpha_2 - \left(1+\alpha_2^2\right)^2}\left[-\left(1+\alpha_2^2\right)\frac{\cos\frac{\theta_1}{2}}{\sqrt{r_1}} + \frac{4\alpha_1\alpha_2}{1+\alpha_2^2}\frac{\cos\frac{\theta_2}{2}}{\sqrt{r_2}}\right] \tag{46}$$

$$\sigma_{xy} = \frac{K_I(V)}{\sqrt{2\pi}}\frac{1+\alpha_2^2}{4\alpha_1\alpha_2 - \left(1+\alpha_2^2\right)^2}\left[2\alpha_1\left(\frac{\sin\frac{\theta_1}{2}}{\sqrt{r_1}} - \frac{\sin\frac{\theta_2}{2}}{\sqrt{r_2}}\right)\right] \tag{47}$$

where, $\alpha_1 = \left(1 - \frac{V^2}{c_1^2}\right)^{1/2}$, $\alpha_2 = \left(1 - \frac{V^2}{c_2^2}\right)^{1/2}$, $\tan\theta_1 = \alpha_1\tan\theta$, $\tan\theta_2 = \alpha_2\tan\theta$, $r_1 = \frac{r\cos\theta}{\cos\theta_1}$, and $r_2 = \frac{r\cos\theta}{\cos\theta_2}$, respectively. From the expression (45)–(47), the relationship between the stress and crack speed is revealed. The crack propagation criterion suggests that the circumferential stress plays an important role in the crack moving process. By transforming the coordinates, the circumferential stress is obtained,

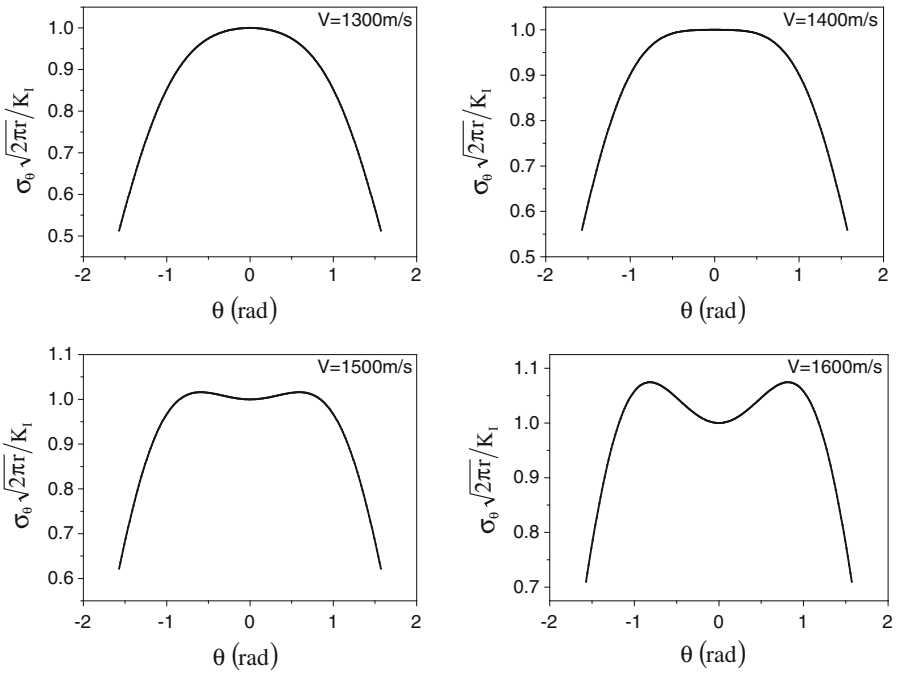

Fig. 7 Curves of $\sigma_\theta\sqrt{2\pi r}/K_I \sim \theta$ on variable propagation speeds

$$\sigma_\theta = \frac{K_I(V)}{\sqrt{2\pi}}\frac{1+\alpha_2^2}{4\alpha_1\alpha_2-\left(1+\alpha_2^2\right)^2}\sin^2\theta\left[(1+2\alpha_1^2-\alpha_2^2)\frac{\cos\frac{\theta_1}{2}}{\sqrt{r_1}}-\frac{4\alpha_1\alpha_2}{1+\alpha_2^2}\frac{\cos\frac{\theta_2}{2}}{\sqrt{r_2}}\right]+\frac{K_I(V)}{\sqrt{2\pi}}\frac{1+\alpha_2^2}{4\alpha_1\alpha_2-\left(1+\alpha_2^2\right)^2}\cos^2\theta\left[-\left(1+\alpha_2^2\right)\frac{\cos\frac{\theta_1}{2}}{\sqrt{r_1}}+\frac{4\alpha_1\alpha_2}{1+\alpha_2^2}\frac{\cos\frac{\theta_2}{2}}{\sqrt{r_2}}\right]+\frac{K_I(V)}{\sqrt{2\pi}}\frac{1+\alpha_2^2}{4\alpha_1\alpha_2-\left(1+\alpha_2^2\right)^2}(-2\sin\theta\cos\theta) \quad (48)$$

In order to analyze it qualitatively, the curves of $\sigma_\theta\sqrt{2\pi r}/K_I \sim \theta$ on variable propagation speeds can be plotted for a given material. For the following given material parameters, $E = 32$ GPa, $\nu = 0.2$, and $\rho = 2450$ kg/m^3, the curves are plotted in Fig. 7. The Rayleigh wave speed of the material is 2119.0m/s.

For a mode I crack, if the crack propagates quasi-statically, the maximum circumferential stress may keep on the original direction of $\theta = 0$. For a dynamic propagating crack, the situation is changed. Figure 7 apparently reveals the change of the normalized circumferential stress distribution at different crack speeds. It can be qualitatively found that when the velocity is low (less than 1,400 m/s), the maximum normalized circumferential stress occurs on the direction of $\theta = 0$, which means the crack propagates along the original direction; while as the velocity increases (beyond 1,500 m/s), the maximum normalized circumferential stress occurs on two symmetrical directions. Based on the viewpoint of the maximum circumferential stress criterion, the crack branching will happen when there exists two symmetrical nonzero directions.

The theory agrees with the fact that dynamic crack branching is related to the crack speed. When the propagation speed is given, it provides a criterion that whether the crack may branch or not. From the analysis of the normalized circumferential stress, we can get the direction in which the maximum occurs. If the speed is not high enough, the direction angle θ equals to zero, otherwise we can get a nonzero angle, which is regarded as the branching angle. Although it is not a physical criterion, it can provide an available criterion in the approximate simulation.

5 Numerical examples

In this section, we apply the method introduced above to model several crack problems that are often used as the benchmarks to validate the capability and accuracy of the method. The first two examples focus on the modeling of static branched cracks and calculation of dynamic stress intensity factor of a semi-infinite crack, respectively. Following this, the dynamic crack branching is simulated for the third example and discussed in detail.

5.1 Static branched cracks

The first example is a static edge crack with branches in a finite plate. As shown in Fig. 8, the right edge of the plate is

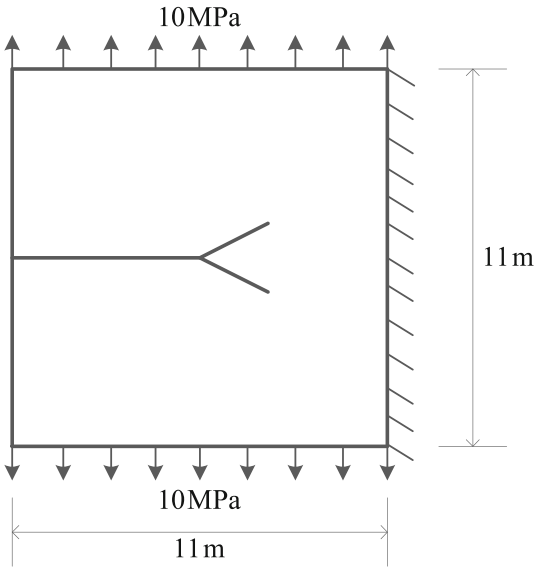

Fig. 8 A plate with the left edge crack and branches

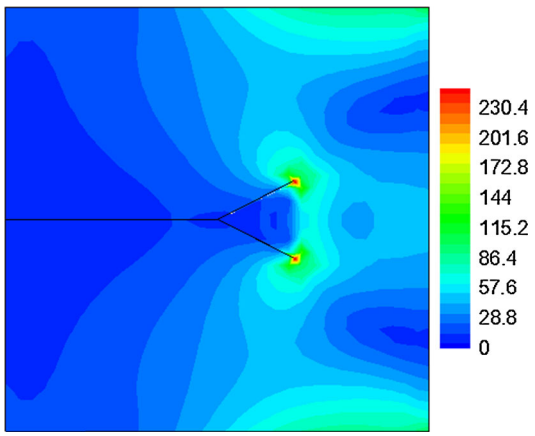

Fig. 9 Mises stress (MPa)

fixed, and uniform tensions are applied on the top and bottom edges. The properties of the material are $E = 210$ GPa and $\nu = 0.3$. With a structure mesh and the XFEM algorithm, the deformed configuration and stress field are obtained as shown in Fig. 9. From the distribution of Mises stress, we can find that there are stress concentrations on both crack tips. At the junction point with three cracks, the stress level is much lower than it at the crack tip location.

Next, we consider a static branched crack in an infinite plate under uniaxial traction as shown in Fig. 10. To have a quantitative study, the stress intensity factors of the three crack tips are calculated. The geometry parameters in the simulation are $\theta = 45°$ and the length ratio $b/a = 1.0$.

In the stress intensity factor (SIF) handbook [33], we can get the theoretical SIF of this problem, which are calculated by the following formulas

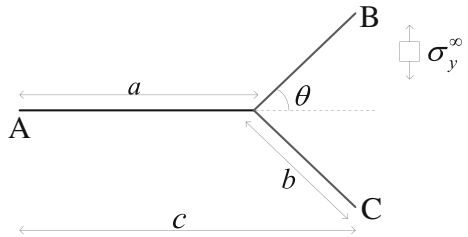

Fig. 10 Geometry of a branched crack in an infinite plate

Table 1 Coefficients of stress intensity factors

	Theoretical	Numerical	Error (%)
F_{IA}	1.044	1.033	1.05
F_{IIA}	0	4.916×10^{-4}	–
F_{IB}	0.5	0.488	2.49
F_{IIB}	−0.5	−0.483	3.40
F_{IC}	0.5	0.489	2.20
F_{IIC}	0.5	0.483	3.40

$$K_{IA} = F_{IA}\sigma\sqrt{\pi\frac{c}{2}}, \quad K_{IIA} = F_{IIA}\sigma\sqrt{\pi\frac{c}{2}} \tag{49}$$

$$K_{IB} = F_{IB}\sigma\sqrt{\pi\frac{c}{2}}, \quad K_{IIB} = F_{IIB}\sigma\sqrt{\pi\frac{c}{2}} \tag{50}$$

$$K_{IC} = F_{IC}\sigma\sqrt{\pi\frac{c}{2}}, \quad K_{IIC} = F_{IIC}\sigma\sqrt{\pi\frac{c}{2}} \tag{51}$$

where $c = a + b\cos\theta$.

In the program, we use the method of interaction integral to calculate the SIF. The coefficient F is calculated from the SIF using Eqs. (49)–(51). The numerical results are compared with the theoretical value, as shown in Table 1. These results agree well with the theoretical solutions.

5.2 Semi-infinite crack in an infinite plate

We choose the second example as a semi-infinite crack in an infinite plate subjected to a tensile stress wave to validate the calculation accuracy of dynamic fracture SIF. The boundary condition is that the left and right edges are fixed in x direction and free in y direction. This is a classical benchmark of the dynamic stress intensity factor calculation. A theoretical solution of this problem is known from Ref. [34], which is compared with our numerical result. Here two main cases are considered, namely a stationary crack and a moving crack under a given speed. The geometry and loading conditions are described in Fig. 11. The stress wave spreads from the top to the crack within the time of $t_c = h/c_d$, where c_d is the dilatational wave speed. The analytical solution is valid only at time $t \leq 3t_c$ when the reflected stress wave reaches the

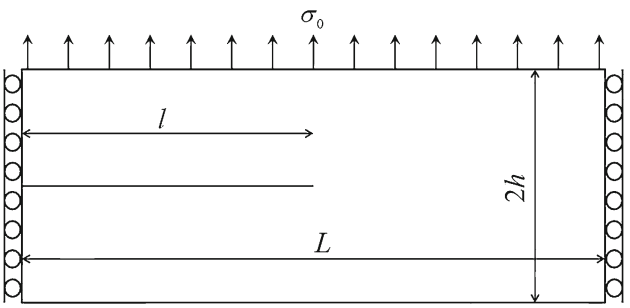

Fig. 11 Geometry and loading for the infinite plate

crack tip. Right after the stress wave reaches the crack tip, the mode I stress intensity factor for a stationary crack can be written as

$$K_I^{\mathrm{dyn}}(0,t) = \frac{2\sigma_0}{1-\nu}\sqrt{\frac{c_d t(1-2\nu)}{\pi}} \tag{52}$$

For a moving crack, we have

$$K_I^{\mathrm{dyn}}(V,t) = k(V)K_I^{\mathrm{dyn}}(0,t) \tag{53}$$

where $k(V)$ is a function of the crack tip speed V,

$$k(V) = \frac{1-V/c_R}{1-V/2c_R} \tag{54}$$

Substituting Eqs. (54) and (52) into Eq. (53), we have

$$K_I^{\mathrm{dyn}}(V,t) = \frac{2\sigma_0}{1-\nu}\sqrt{\frac{c_d t(1-2\nu)}{\pi}}\frac{1-V/c_R}{1-V/2c_R} \tag{55}$$

To obtain the numerical results, we choose the plate dimensions as $h = 2$ m, $L = 10$ m and $l = 5$ m, the material properties $E = 210$ GPa, $\nu = 0.3$ and $\rho = 8000$ kg/m^3. The tensile stress σ_0 is 500 MPa. The dilatational wave speed of the material is 5944.5 m/s and the corresponding Rayleigh wave speed is 2859.7 m/s.

For a stationary crack, the crack does not propagate during the calculation. The load is applied at $t = 0$. The mode I SIF is normalized by $\sigma_0\sqrt{h}$ and the time is normalized by t_c. Various mesh densities are used to check the numerical convergence. The simulation results are compared with the theory solutions as shown in Fig. 12.

The numerical results have an oscillation near the theoretical solution and all the three meshes give satisfying results. It reveals that the program has the capacity to obtain the dynamic stress intensity factor for a stationary crack. Figure 13 exhibits the Mises stress field of the plate for different times during the spread process of stress wave. The evolution of stress field is described apparently.

For the moving crack condition, the crack starts to propagate at $1.0t_c$ or $1.5t_c$, respectively, as shown in Fig. 14. The crack speed is given as 1,980 m/s. If the crack starts to propagate at $1.0t_c$, the stress intensity factor keeps at a low level before the time $1.0t_c$, while after that the SIF increases at a

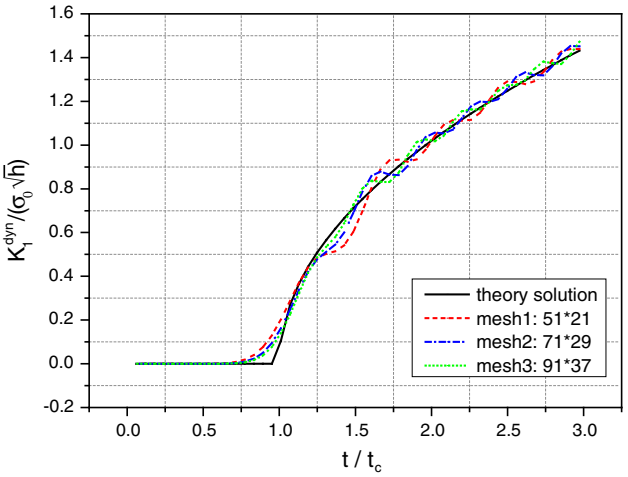

Fig. 12 Stress intensity factor for a stationary crack

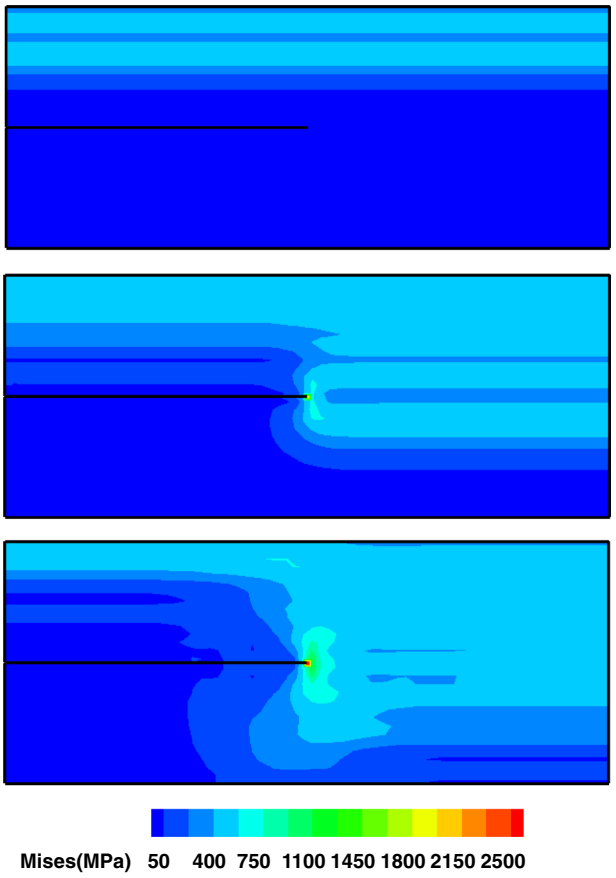

Fig. 13 Mises stress fields (MPa) (200, 500, 800 μs)

lower level than that for a stationary crack. On the contrary, if the crack starts to propagate at $1.5t_c$, the SIF increases as the case for a stationary crack before the crack moves. After the time $1.5t_c$, the SIF drops to a lower level. The numerical results seize the feature of both processes, and have a good agreement with the theoretical solutions.

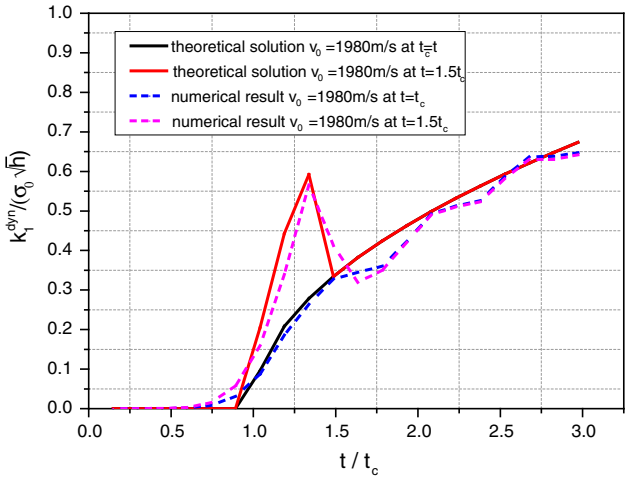

Fig. 14 Stress intensity factors for moving cracks with a given speed

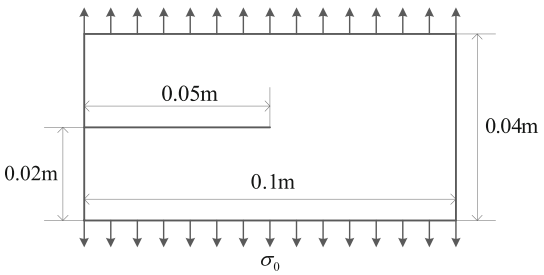

Fig. 15 Schematic of the crack branching model

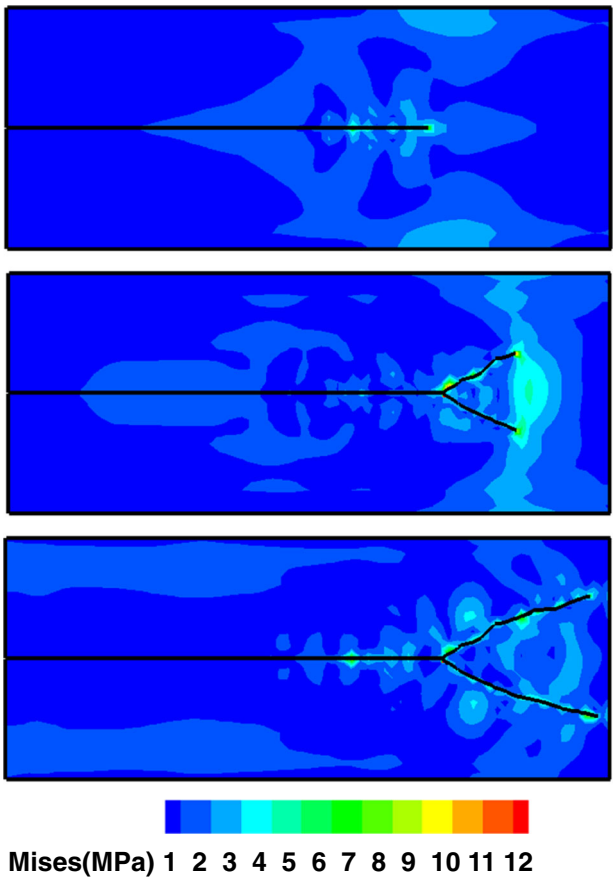

Fig. 16 Crack branching paths (25, 35, 45 μs)

5.3 Dynamic crack branching

The third example concerns a crack propagation in a pre-notched specimen as shown in Fig. 15. The dimension of specimen is 0.1 × 0.04 m, and the length of initial crack is 0.05m. The properties of material are $E = 32$ GPa, $\nu = 0.2$ and $\rho = 2,450$ kg/m^3. The dilatational wave speed is $c_d =$ 3809.5m/s and the shear wave speed $c_s = 2332.8$ m/s. The corresponding Rayleigh wave speed is $c_R = 2119.0$ m/s. Tensile tractions $\sigma = 1$ MPa are applied on the top and bottom edges as a step function in time. The numerical results of this problem are given by Belytschko et al. [24], Song et al. [21] and Borden et al. [18], respectively. The experimental results with different dimensions are available in Refs. [2,6, 35–37].

In the experiments, the crack propagates along the original straight direction with increasing crack speed before branching. When the speed reaches the critical value, the crack branching occurs. Besides the main branches, some secondary micro branches are also observed. In our simulation, the quadrilateral elements are used. The maximum circumferential stress criterion is used to obtain the crack growth paths and the theory introduced in Sect. 4 is used to predict the crack branching. The solution given by Yoffe is established under some assumptions which are very difficult to be satisfied practically. Here we just use it as estimation for branching initiation.

The propagation paths and Mises stress fields obtained from the simulation are shown in Fig. 16. The crack starts to propagate at about 8 μs, which is a typical mode I crack. The initial crack grows along the original direction until the branching criterion is reached. The single crack becomes two branches when crack branching takes place at about 25 μs. After that time, the two branches continue to propagate separately.

Based on the stress fields, we use the method of interaction integral to calculate the SIF during the crack propagation. The dynamic SIF is $3.851K_{\mathrm{Ic}}$ when the crack branching occurs. This condition is stronger than the assumption that crack branching takes place when the energy release rete G attains the integer multiplies of value G_{c} required for crack initiation, for example, $G = 2G_{\mathrm{c}}$ when a single crack becomes two.

Figure 17 exhibits the crack propagation speed obtained from the simulation. The speed reaches the maximum value just before the branching. The ratio of the maximum crack speed to Rayleigh wave speed is 0.741, which is also higher than that of 0.4 obtained from the experiment [6]. The error

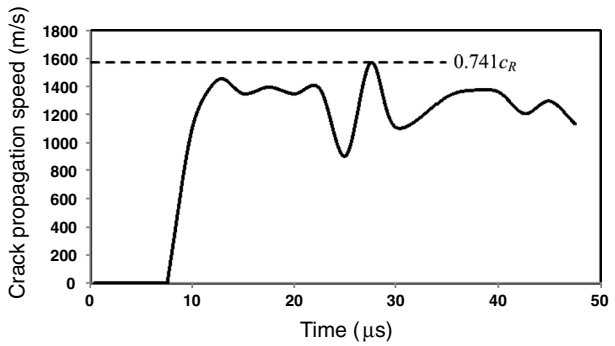

Fig. 17 Crack propagation speed

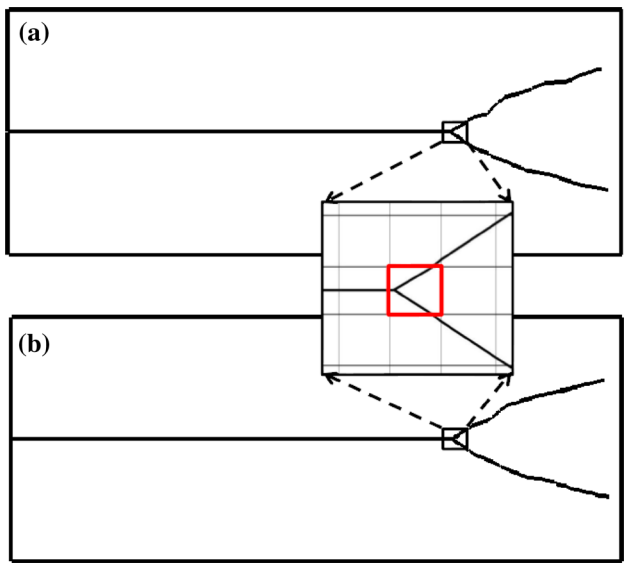

Fig. 18 Comparison of the crack propagation paths: **a** Enriched **b** Simplified

may be partially attributed to the branching criterion used in the simulation, since the critical velocity established from Yoffe's solution is higher than that observed in the experiment.

In the simulations, we consider the enrichment method for an element embedded by a junction or an element crossed by two separated cracks as described in Sect. 2.3. However, in the previous studies of this example, the branching process is often simulated by the simply deleted element method when the branching occurs. Here we compare the crack paths for these two different treatments. The element deletion is realized by ignoring the stiffness and nodal force contribution for the branched elements, so that the complicated enrichment and integration is avoided inside the element (the element in a small red rectangular as shown in Fig. 18). But for matching the degrees of freedom with the neighboring elements and the post-process, the geometry description of the discontinuities is remained inside these kinds of elements. The results obtained by the simplified treatment are compared with the results with enrichment as shown in Fig. 18. We can find the similar branching configurations, which are mainly determined by the status before branching, so the simplification does not change the branching path a lot. By the way, it is worth mentioning that the roughness of the crack surface and micro branches observed in the experiments are ignored in the numerical simulation.

6 Conclusions

The new methodology and program based on XFEM is developed in this paper to simulate dynamic crack propagation and branching. The enrichments for a branched crack are developed. We focus on introducing the enrich scheme of the element crossed by two separated cracks and the element embedded by a junction. More enriched degrees of freedom are needed in these two kinds of elements because of the additional discontinuities inside the element. The new enrichment makes it possible to model branched cracks with structure meshes.

The mass lumping technique based on the shifted enriched shape function is developed to improve the efficiency of simulation. It follows a principle of kinetic energy conservation in the special motion modes. The mass matrix of an element contained two strong discontinuities is deduced and a new node mass assignment technique is carried out based on the subdomain integral weight.

The crack speed is used as the criterion of crack branching. The process of a crack propagation and branching is modeled. The results including the branching angle and propagation path are compared with conventionally used element deletion method. The branching theory used in this paper is only a criterion of the branching initiation. The problem of dynamic crack branching is still an open question. The further study needs to be carried out in the near future.

Acknowledgments This work is supported by the National Natural Science Foundation of China under Grant No. 11372157 and The Special Research Grant for Doctor Discipline by Ministry of Education of China under Grant No. 20120002110075

References

1. Ravi-Chandar K, Knauss WG (1984) An experimental investigation into dynamic fracture-III. On steady-state crack propagation and crack branching. Int J Fract 26:141–154
2. Sharon E, Gross S, Fineberg J (1995) Local crack branching as a mechanism for instability in dynamic fracture. Phys Rev Lett 74:5096–5099. doi:10.1103/PhysRevLett.74.5096
3. Boudet JF, Ciliberto S, Steinberg V (1996) Dynamics of crack propagation in brittle materials. J Phys II France 6:1493–1516. doi:10.1051/jp2:1996144
4. Fliss S, Bhat HS, Dmowska R, Rice JR (2005) Fault branching and rupture directivity. J Geophys Res 110:B06312. doi:10.1029/2004jb003368

5. Bhat HS, Olives M, Dmowska R, Rice JR (2007) Role of fault branches in earthquake rupture dynamics. J Geophys Res 112:B11309. doi:10.1029/2007jb005027
6. Fineberg J, Sharon E (1999) Confirming the continuum theory of dynamic brittle fracture for fast cracks. Nature 397:333–335. doi:10.1038/16891
7. Yoffe EH (1951) The moving Griffith crack. Philos Mag 42:739–750. doi:10.1080/14786445108561302
8. Eshelby JD (1999) Energy relations and the energy-momentum tensor in continuum mechanics. Fundamental Contributions to the Continuum Theory of Evolving Phase Interfaces in Solids. 82–119. doi:10.1007/978-3-642-59938-5_5
9. Adda-bedia M (2005) Brittle fracture dynamics with arbitrary paths III. The branching instability under general loading. J Mech Phys Solids 53:227–248. doi:10.1016/j.jmps.2004.06.001
10. Martín T, Español P, Rubio MA (2005) Mechanisms for dynamic crack branching in brittle elastic solids: strain field kinematics and reflected surface waves. Phys Rev E 71:036202. doi:10.1103/PhysRevE.71.036202
11. Katzav E, Adda-Bedia M, Arias R (2007) Theory of dynamic crack branching in brittle materials. Int J Fract 143:245–271. doi:10.1007/s10704-007-9061-x
12. Zhou SJ, Lomdahl PS, Thomson R, Holian BL (1996) Dynamic crack processes via molecular dynamics. Phys Rev Lett 76:2318–2321. doi:10.1103/PhysRevLett.76.2318
13. Bolander JE Jr, Saito S (1998) Fracture analyses using spring networks with random geometry. Eng Fract Mech 61:569–591
14. Xu X-P, Needleman A (1994) Numerical simulations of fast crack growth in brittle solids. J Mech Phys Solids 42:1397–1434
15. Ha YD, Bobaru F (2010) Studies of dynamic crack propagation and crack branching with peridynamics. Int J Fract 162:229–244. doi:10.1007/s10704-010-9442-4
16. Rabczuk T, Song J-H, Belytschko T (2009) Simulations of instability in dynamic fracture by the cracking particles method. Eng. Fract. Mech. 76:730–741. doi:10.1016/j.engfracmech.2008.06.002
17. Henry H (2008) Study of the branching instability using a phase field model of inplane crack propagation. Europhys Lett 83:16004. doi:10.1209/0295-5075/83/16004
18. Borden MJ, Verhoosel CV, Scott MA, Hughes TJR, Landis CM (2012) A phase-field description of dynamic brittle fracture. Comput Methods Appl Mech Eng. 217–220:77–95. doi:10.1016/j.cma.2012.01.008
19. Belytschko T, Black T (1999) Elastic crack growth in finite elements with minimal remeshing. Int J Numer Methods Eng 45:601–620
20. Moës N, Dolbow J, Belytschko T (1999) A finite element method for crack growth without remeshing. Int J Numer Methods Eng 46:131–150
21. Song J-H, Areias PMA, Belytschko T (2006) A method for dynamic crack and shear band propagation with phantom nodes. Int J Numer Methods Eng 67:868–893. doi:10.1002/nme.1652
22. Duan QL, Song J-H, Menouillard T, Belytschko T (2009) Element-local level set method for three-dimensional dynamic crack growth. Int J Numer Methods Eng 80:1520–1543. doi:10.1002/nme.2665
23. Daux C, Moës N, Dolbow J, Sukumar N, Belytschko T (2000) Arbitrary branched and intersecting cracks with the extended finite element method. Int J Numer Methods Eng 48:1741–1760
24. Belytschko T, Chen H, Xu J, Zi G (2003) Dynamic crack propagation based on loss of hyperbolicity and a new discontinuous enrichment. Int J Numer Methods Eng 58:1873–1905. doi:10.1002/nme.941
25. Song J-H, Wang H, Belytschko T (2007) A comparative study on finite element methods for dynamic fracture. Comput Mech 42:239–250. doi:10.1007/s00466-007-0210-x
26. Song J-H, Belytschko T (2009) Cracking node method for dynamic fracture with finite elements. Int J Numer Methods Eng 77:360–385. doi:10.1002/nme.2415
27. Zhuang Z, Cheng BB (2011) Development of X-FEM methodology and study on mixed-mode crack propagation. Acta Mech Sin 27:406–415. doi:10.1007/s10409-011-0436-x
28. Zhuang Z, Cheng BB (2011) Equilibrium state of mode-I subinterfacial crack growth in bi-materials. Int J Fract 170:27–36. doi:10.1007/s10704-011-9599-5
29. Stolarska M, Chopp DL, Moës N, Belytschko T (2001) Modelling crack growth by level sets in the extended finite element method. Int J Numer Methods Eng 51:943–960
30. Fries T-P, Belytschko T (2010) The extended/generalized finite element method: an overview of the method and its applications. Int J Numer Methods Eng 84:253–304. doi:10.1002/nme.2914
31. Zi G, Song J-H, Budyn E, Lee S-H, Belytschko T (2004) A method for growing multiple cracks without remeshing and its application to fatigue crack growth. Model Simul Mater Sci Eng 12:901–915. doi:10.1088/0965-0393/12/5/009
32. Menouillard T, Réthoré J, Combescure A, Bung H (2006) Efficient explicit time stepping for the eXtended finite element method (X-FEM). Int J Numer Methods Eng 68:911–939. doi:10.1002/nme.1718
33. Chinese Aeronautical Establishment (1981) Stress intensity factor handbook (in Chinese). Science press, Beijing
34. Freund LB (1990) Dynamic fracture mechanics. Cambridge monographs on mechanics and applied mathematics. Cambridge University Press, Cambridge
35. Sharon E, Fineberg J (1996) Microbranching instability and the dynamic fracture of brittle materials. Phys Rev B 54:7128–7139. doi:10.1103/PhysRevB.54.7128
36. Ramulu M, Kobayashi AS (1985) Mechanics of crack curving and branching—a dynamic fracture analysis. Int J Fract 27:187–201
37. Ravi-Chandar K (1998) Dynamic fracture of nominally brittle materials. Int J Fract 90:83–102